








Tungsten erosion by unipolar arcing in DIII-D

I Bykov¹ , C P Chrobak² , T Abrams² , D L Rudakov^{1, 3} ,
W R Wampler⁴, E M Hollmann¹, R A Moyer¹ , J A Boedo¹ , B Stahl²,
E T Hinson⁵ , J H Yu¹ , C J Lasnier⁶, M Makowski⁶ and A G McLean⁶

¹ University of California (San Diego), La Jolla, CA United States of America

² General Atomics, PO Box 85608, San Diego, CA 92186-5608, United States of America

³ Oak Ridge National Laboratory, Oak Ridge, TN 37830, United States of America

⁴ Sandia National Laboratories, Albuquerque, NM, and Livermore, CA, United States of America

⁵ University of Wisconsin-Madison, Wisconsin, WI 53706, United States of America

⁶ Lawrence Livermore National Laboratory, Livermore, CA 94550, United States of America

E-mail: ibykov@ucsd.edu

Received 6 June 2017, revised 25 August 2017

Accepted for publication 21 September 2017

Published 20 October 2017



CrossMark

Abstract

Unipolar arcing was an important mechanism of metal surface erosion during the recently conducted Metal Rings Campaign in DIII-D when two toroidally continuous tile rings with 5 cm wide W-coated TZM inserts were installed in graphite tiles in the lower divertor, one on the floor and one on the shelf. Most of the arc damage occurred on the shelf ring. The total amount of W removed by arcing from the affected $\sim 4\%$ of the shelf ring area was estimated $\sim 0.8 \times 10^{21}$ at., about half of the total amount of W eroded and redeposited outside the inserts $(1.8 \pm 0.9) \times 10^{21}$ at. The rings were exposed for a total of ~ 480 discharges, an equivalent of plasma time on W surfaces (with $I_p > 0.5$ MA) $\sim 10^3$ s. Arcing was monitored *in situ* with WI (400.9 nm) filtered camera and photomultipliers and showed that: (i) arcing only occurred during ELMs and disruptions, (ii) arcing rate was much lower on the floor than on the shelf ring, and (iii) arcing had a low cut off power flux density about 2 MW m^{-2} . About half of arc tracks had large 10° pitch angle and probably were produced during disruptions. Such tracks were only found on the shelf. Moderate toroidal variation of the arc track density and W erosion with nearly $n = 1$ pattern has been measured.

Keywords: DIII-D, arcing, tungsten, erosion

(Some figures may appear in colour only in the online journal)

1. Introduction

Unipolar arcs are electric discharges between a material surface acting as the cathode and the plasma acting as the anode. Arcing is an important local surface erosion mechanism in controlled fusion devices [1]. Arcing is routinely observed in machines with graphite first wall but owing to the high sputtering and chemical erosion of C it usually is not the dominant mechanism [2]. In machines with metal first wall aiming at reduced plasma contamination and wall erosion by atomic sputtering, arcing can be a much stronger local erosion source. It was demonstrated more than 40 years ago that under edge plasma conditions unipolar arcing can lead to several orders of magnitude higher erosion rates than simple atomic sputtering [3]. This makes arcing of primary concern

for future fusion devices with high-Z wall like ITER and DEMO when the wall impurity source has to be minimized.

In present day experiments arcing is not an issue for tokamak operation but can contribute to plasma contamination and complicate interpretation of *in situ* and campaign integrated erosion measurements. Still, there is no arc avoidance strategy proposed compatible with high-performance tokamak operation. Arcing has been studied in many machines, either in dedicated experiments with small-scale test samples exposed in a limited number of discharges with controlled parameters [4–6], or by performing shutdown in-vessel surveys of permanently installed components assessing integrated effect of arcing after the whole campaign [2, 7]. In June–July 2016, a short-term Metal Rings Campaign (MRC) was conducted at DIII-D to study W sourcing in the divertor,

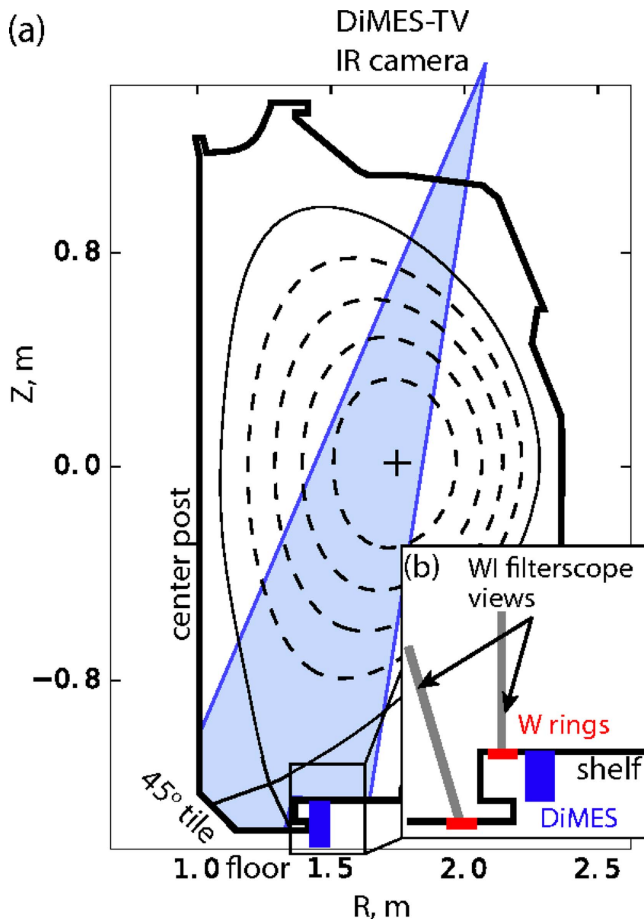


Figure 1. Schematic view of the DIII-D poloidal cross section showing location of the divertor-viewing cameras and their accessible areas (a). (b) shows locations of the shelf and floor W rings, DiMES, and WI filterscopes' chords (b).

W migration, transport, and core contamination, and to explore high-Z wall compatibility with high performance plasmas [8, 9]. In this work, we report on observations of arcing on metal surfaces and their effect on material erosion in the divertor of DIII-D during operations with partially W-covered divertor plasma facing components (PFCs).

2. Experimental

DIII-D is a divertor tokamak with minor radius $a = 0.67$ m and major $R = 1.67$ m [10], with PFCs made of ATJ graphite conditioned by periodic boronizations. For MRC, two toroidally continuous 5 cm wide W-coated TZM (Mo alloy with 0.50% Titanium and 0.08% Zirconium) tile inserts (rings) have been installed on the floor near the pump entrance and on the shelf. The floor insert was coated by W using chemical vapor deposition (CVD) of WF_6 gas. Measurements on a test sample showed $\sim 12 \mu\text{m}$ layer thickness. The shelf insert was coated by W using electron-beam induced physical vapor deposition (PVD), with the layer thickness $1.5 \pm 0.5 \mu\text{m}$.

Figure 1 schematically shows an outline of the DIII-D first wall, locations of divertor diagnostics, W rings and Divertor Materials Evaluation Station (DiMES) [11]. DiMES

allows up to $\varnothing 5$ cm sample exposure flush with the lower divertor surface and sample exchange on inter-shot time scale. For more details see figure 1 in [12]. Measurement of infrared (IR) emission in the range $3\text{--}5 \mu\text{m}$ was done with an IR camera on a graphite divertor section without a W insert. This data was used for calculation of radial distribution of incident heat flux q_{\perp} . The camera was operated in fast line-scan mode with framing rate up to 12 kHz thus able to capture heat flux evolution during ELMs. The inserts near DiMES were imaged with a WI-filtered (400.9 nm) DiMES-TV camera with framing rate 100 Hz and exposure time 10 ms [13]. Filtered photo multipliers (filterscopes) with sampling rate 5×10^4 Hz have been installed to monitor each of the W rings (two nearby chords with $\varnothing 2$ cm per ring) and provide background subtracted photon fluxes of neutral W line at 400.9 nm using a recently implemented technique [14].

3. Results and discussion

3.1. In situ arc detection

The Metal Rings Campaign spanned a total of ~ 480 discharges ($I_p > 0.5$ MA) with integrated exposure of the W surfaces to diverted plasma 350 s on the shelf and 660 s on the floor. Most of the discharges were in H-mode with attached OSP placed on either of the two rings. About 20% of developed H-mode discharges terminated by a disruption.

WI filterscopes detected peaking of the W source during various transient events which could be due to arcing or sputtering. Since arcing is spatially localized and sputtering source must be nearly the same for two nearby filterscope chords, we used the differential signal from two nearby WI filterscopes on each ring to detect arcing. One of the shelf filterscopes' spots was within the camera field of view, see figures 2, 4 and the camera was used to validate this technique. With this we confirmed that arcing only occurred during ELMs and during disruptions.

Quantitative measurements of arcing rate (number of arcs per cm^2 per ELM) was possible with the DiMES-TV camera. In H-mode during ELMs, multiple arcing events were detected on the shelf ring with much lower rate on the floor ring also in agreement with the filterscopes' data. Excluding disruptions, large infrequent ELMs with high q_{\perp} at either the end of ELM-free phases or RMP ELM-suppressed periods were causing the most intense arcing. An example of a camera frame capturing arcing during an ELM is shown in figure 2. The tracks are aligned radially owing to the small radial B -field component (see the discussion below). Notably, with OSP on the floor ring all the arcs are seen on the shelf. This strong asymmetry was typical for the whole campaign and probably had following reasons.

- Under otherwise similar conditions, arcing was more likely for the thinner W coating on the shelf. This trend is common for other experiments. For example, in AUG with full W divertor arcing was reported on the inner marker Tile 5 (inboard from ISP) with W coverage

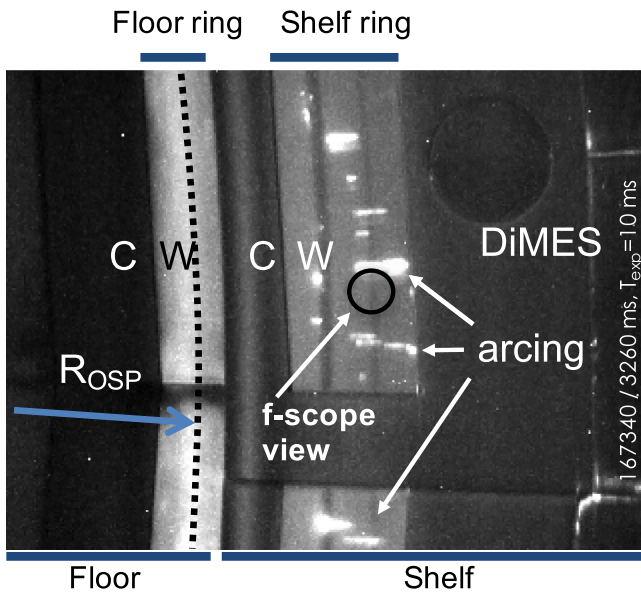


Figure 2. Example of arcing on W during an ELM crash. OSP is on the floor ring but arcing is only seen on the shelf. Some wall elements and WI filterscope collection area are shown. In diverted discharges the arcs propagate in the $\vec{B} \times \vec{J}_{arc}$ direction nearly radially because the radial B -field component is small, leading to pitch angle $\sim 3^\circ$.

~ 300 nm [15] as compared with no arcing on 500–600 nm marker layers in the outer divertor and $1.5 \mu\text{m}$ under OSP. In previously reported DIII-D studies of metals' erosion on DiMES arcing was observed on ~ 100 nm thick W layer on graphite [6]. At the same time, no arcing occurred on 1.6 mm thick W DiMES inserts exposed in various H-mode OSP conditions in [16].

- With OSP on the floor ring, broadening of the strike point footprint during ELMs led to more similar conditions (deposited heat flux q_{\perp} , N_e and T_e) on both rings, while with OSP on the shelf ring the floor ring was always in the low N_e and T_e private flux region. In the shown example the arcing occurred on the shelf ring in the SOL at $\psi_n \approx 1.04$ during a large ELM with heat flux nearly similar on both floor and shelf rings 5 MW m^{-2} .

Ignition and burn conditions for an arc include a sufficiently high potential drop across the sheath (a function of T_e) exceeding the arc voltage (of the order 20 V [17]). N_e can influence arc ignition through controlling the sheath width and electrostatic field near the surface. Additionally, surface conditions such as roughness, temperature, presence of dielectric layers, inclusions and impurities are important [18]. ELM resolved measurements of N_e and T_e near the W rings were not possible. Instead, as a predictor parameter for the arcing rate, we proposed to use the deposited heat flux density $q_{\perp} \sim N_e T_e^{3/2}$ measured with high temporal and spatial resolution by the IR camera. Maximum arcing rates on W surfaces were counted using DiMES-TV images and plotted as function of intra-ELM q_{\perp} , figure 3. For a given q_{\perp} a count rate of zero means that no arcing was detected during many

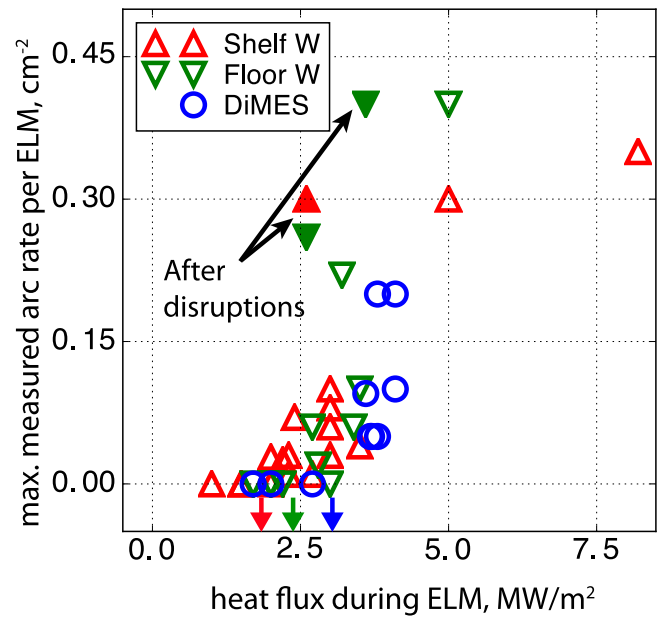


Figure 3. Maximum measured areal density of arcs per ELM versus peak intra-ELM heat flux on the W rings during MRC and in a separate experiment on DiMES with sample surface similar to the shelf ring. The colored arrows indicate the threshold q_{\perp} for each case. The filled points were measured in discharges after disruptions.

ELMs with similar q_{\perp} . The non-zero counts correspond to maximum observed arcing rate in individual ELMs. The lower ELM-power threshold for each case was obtained by linear extrapolation of the non-zero rate data, marked by colored arrows in figure 3. Arcing on the shelf insert had threshold $\sim 1.8 \text{ MW m}^{-2}$ versus $\sim 2.4 \text{ MW m}^{-2}$ on the floor owing probably to its lower thickness and/or different coating method (PVD on the shelf versus CVD on the floor). Additional data are available from a separate DiMES experiment prior to MRC [19] where a $\varnothing 5$ cm sample with surface similar to the shelf ring was exposed in ~ 20 discharges. The DiMES surface has even higher than the floor ring arcing threshold at $\sim 3 \text{ MW m}^{-2}$. This is probably because the DiMES sample did not experience disruptions and thus avoided surface contamination which could lead to increased arcing rates. This argument is supported by the observation that in a series of discharges following disruptions the arcing rate increased on the floor ring to 0.4 cm^{-2} at $q_{\perp} = 3.6 \text{ MW m}^{-2}$ and on the shelf to 0.3 cm^{-2} at $q_{\perp} = 2.6 \text{ MW m}^{-2}$, see figure 3. In a series of discharges following a disruption the surfaces clean up and the arcing rates drop to their typical values. This is in agreement with the results from an arc simulator [20] and other tokamaks, see [18] and references therein. In all scenarios there was no detectable arcing between ELMs or in L-mode, in agreement with a previously reported correlation between transient events and the arcing rates [7, 21, 22]. During disruptions, the W-filtered camera saturated while the WI filterscopes showed intense arcing. Evidence of disruption-induced arcing was also found during post mortem analysis as discussed below.

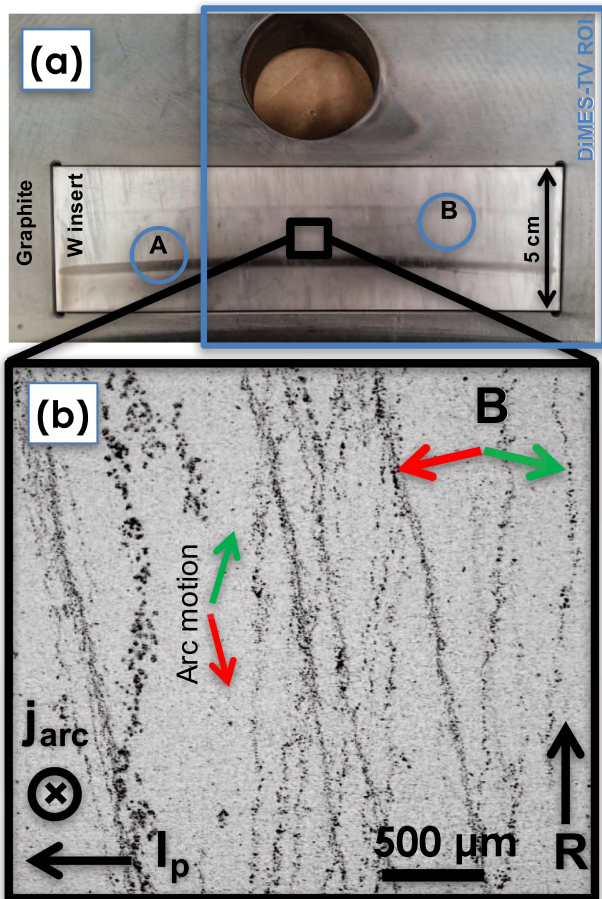


Figure 4. (a) Post mortem overview of the shelf insert near DiMES. Two WI filterscope spots' projections are shown with circles A and B. Part of the image inside the blue frame is also seen by DiMES-TV camera. Multiple arc tracks with different pitch angle are visible. (b) SEM close up with indication of I_p , normal and reversed B_r , and arc current. The respective arc motion directions are indicated for tracks with high pitch angle $\sim 10^\circ$.

3.2. Post mortem tile analysis

The full sets of tiles with the metal inserts and some of the graphite divertor tiles including those from the 45° tile were removed from the vessel after the experiment for post mortem analysis. This included electron microscopy (SEM) with x-ray micro analysis and x-ray fluorescence analysis (XRF). The latter technique is implemented with a hand held XRF spectrometer with the beam $\varnothing 5$ mm and energy up to 40 keV. It is used to measure in-vessel distributions of medium- to high-Z elements [23].

On the shelf insert multiple arc tracks were visible by unaided eye. The floor insert had over factor 10 fewer arc tracks which was also confirmed by visible and electron microscopy. Figure 4(a) shows a post mortem image of the shelf insert near DiMES with multiple arc tracks. The dark line on the W insert is due to C deposition during operation with reversed B_r , this C has not been re eroded in recessed surface areas. Arc damage was predominantly found on the shelf inserts, therefore analysis focused on the tracks found on the shelf rings. Arc tracks on bare W microscopically consist

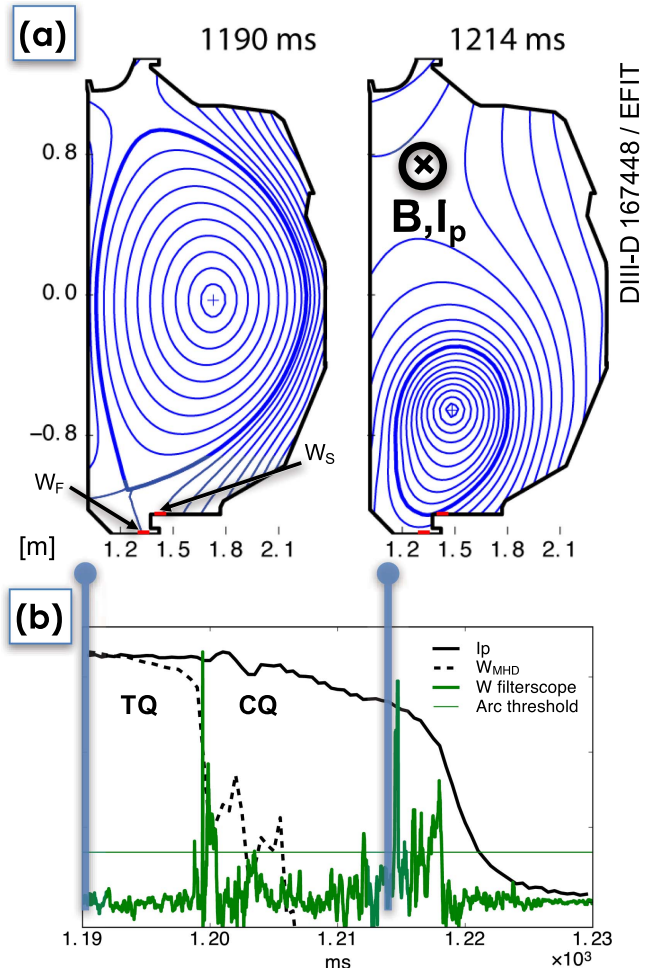


Figure 5. (a) EFIT reconstruction of downward plasma motion during a VDE disruption. The shelf with the W_s insert receives high heat flux but shadows the floor ring W_f . (b) Disruption evolution of plasma current I_p , stored energy W_{MHD} , and differential WI filterscope signal on the shelf. The latter has multiple peaks between thermal (TQ) and current quench (CQ)—a signature of intense arcing.

of individual holes about $\varnothing 10 \mu\text{m}$ (Type I, see [17]) and in areas partly covered by redeposited C they are continuous (Type II) and about 1 cm long.

In presence of strong magnetic field parallel to the surface the arcs are known to move in the *retrograde* direction $\vec{B} \times \vec{J}$ i.e. opposite to the direction of Lorenz force on net arc current [1, 17]. This property makes it possible to reconstruct the local B -field direction at the time when arc tracks appeared. Two kinds of tracks can be seen in figure 4(b): nearly radial with pitch angle of a few degrees, and with pitch angle about 10° . The low-pitch tracks must have appeared during controlled phases of diverted discharges when the field line pitch angle is small. Tracks with the angle $\sim 10^\circ$ must be due to disruptions, similar to experiment [4]. The two preferential inclinations are due to forward and reversed B_r .

Equilibrium evolution during a vertical displacement event (VDE) [24], a disruption typical for MRC, was calculated with fast EFIT [25], see figure 5(a). As the VDE develops, the shelf nose starts acting as a toroidal limiter

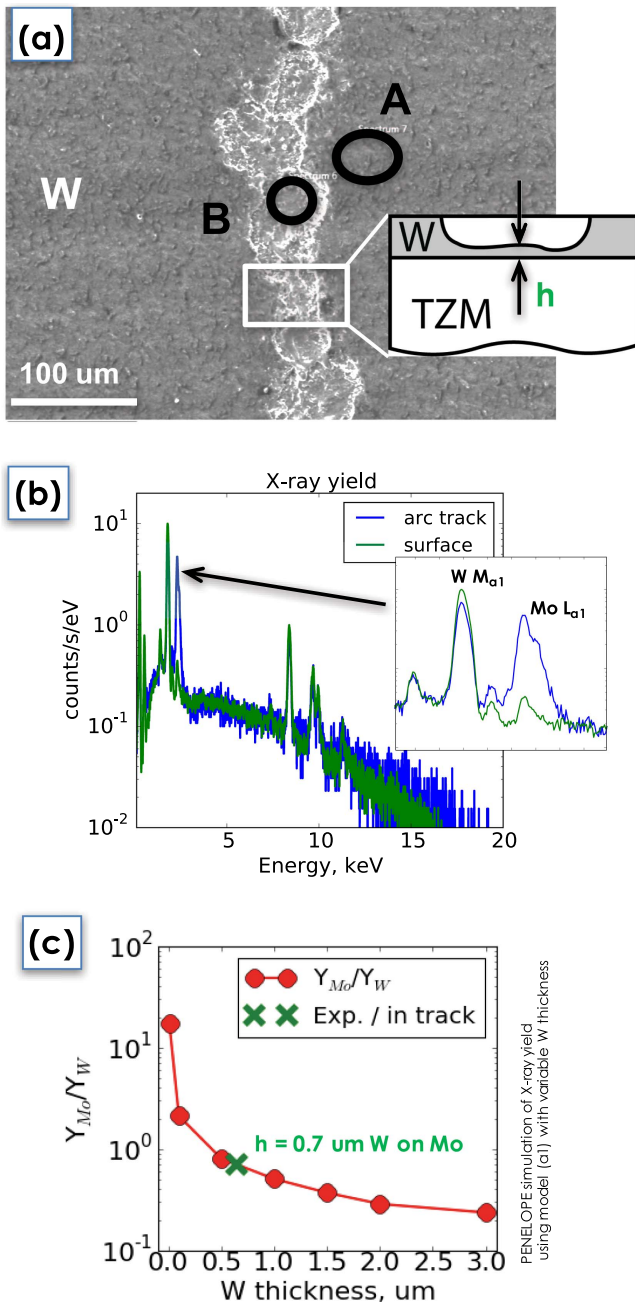


Figure 6. (a) Example of an arc track on the shelf W insert. X-ray spectra in (b) have been collected from regions A and B and relative Mo and W yield from B was matched by PENELOPE [26] simulation in (c) at assumed W layer thickness $0.7 \mu m$.

shadowing the floor, hence no damage on the floor ring. The two major WI peaks in figure 5(b) coincide with the early thermal quench and the final current quench. Between these two events the field-line pitch angle in the middle of the shelf ring increases from 3° to 7° which explains the high pitch angle arc tracks. About half of the total number of arc tracks were due to disruptions.

An important quantity is the total amount of W eroded by arcing. It can be estimated if the total arc-damaged area and the fraction of the removed W layer are known. Figure 6(a)

shows a SEM image of an arc track on the shelf insert. The x-ray spectra in (b) have been collected using a 20 keV e-beam from regions indicated by circles A (in the arc track) and B (on undamaged surface). The W x-ray yield does not disappear at the bed of the track (Region B) which means that the arc did not burn through the whole W layer or at least some W was not removed. To find thickness of the remaining W layer the relative intensity of the most prominent in this range lines $W M_{\alpha 1}$ and $Mo L_{\alpha 1}$ has been simulated with PENELOPE Monte Carlo code for coupled electron–photon transport [26]. A simple geometry with thick elemental Mo substrate and top W layer (a proxy of shown in inset (a1) of figure 6) of varied thickness was used for simulation. Figure 6(c) shows the results of this simulation for W layer thickness up to $3 \mu m$. The calculated relative x-ray yield is best matched with the measured at model W layer thickness $0.7 \mu m$. Thus, on average $0.8 \mu m$ of W has been removed from the $1.5 \mu m$ thick W layer.

Fractional area of the arc-damaged surface is measured using low magnification SEM images like in figure 4(b). They show good contrast between damaged (dark pixels) and non-damaged regions. Relative pixel counts lead to an estimate of about 4% fractional area damaged by arcing. Extrapolating to the total area of the shelf ring this amounts to $160 cm^2$ and total removed 0.8×10^{21} at. W. This is about half of the total W redeposited poloidally outside the W rings (and thus net eroded) measured by XRF—550 mg or $(1.8 \pm 0.7) \times 10^{21}$ at. W [23].

It is not possible to conclude where the W eroded by arcing was transported. Multiple micron-sized W droplets were found around the tracks but could not account for the total amount of removed W. Fast droplets ejected by arcing can potentially penetrate much deeper into the edge plasma and even cross the separatrix and add to the core W contamination. Because arcing also occurs on W surfaces outside the view of relevant diagnostics, we could not compare similar ELM discharges with and without arcing to conclude whether or not there is higher core W content in the former case. This has to be studied in future experiments using e.g. localized W source on DiMES and a set of core W diagnostics.

The analysis presented so far focused on data from a single toroidal location near DiMES at 150° . It is important to verify to what extent this analysis is representative of the whole divertor. Figure 7 shows toroidal distribution of the arc count rate on all the shelf inserts sorted by the arc track density and binned in 5 groups. The minimum value is about 50% of the maximum. The area near the DiMES insert shows high arc track density but the DiMES insert has about average value. The $n \approx 1$ structure of the distribution may be a result of an $n = 1$ error field effect on the radial profiles at different toroidal locations affecting both the arc rate and the net erosion. This hypothesis can not be further substantiated. Presence of C spacers and diagnostic ports breaking toroidal continuity of the W surface could increase W surface contamination by redeposition in the typical downstream direction (toward higher toroidal angles) and promote arcing.

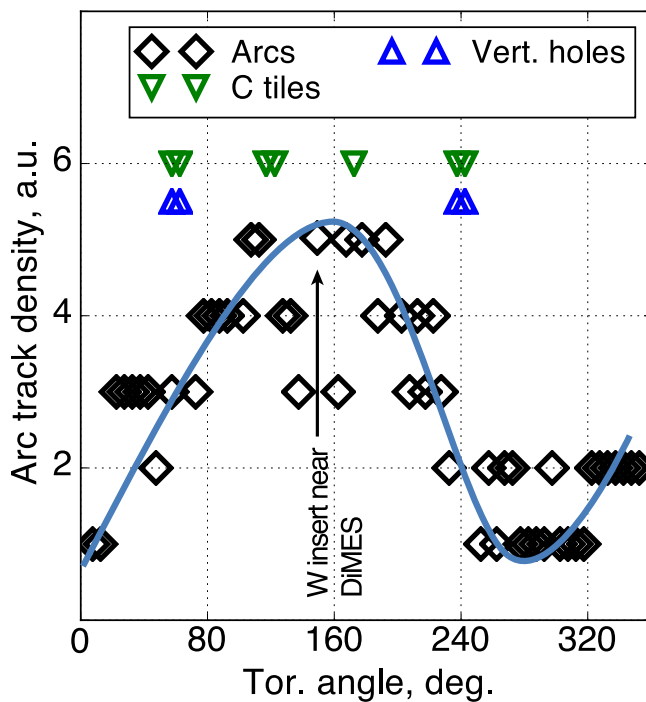


Figure 7. Toroidal distribution of arc track density on the shelf W ring with $n \approx 1$ pattern (the line is to guide the eye). The maximum of the distribution falls near the location of C tiles with discontinuous W coverage and with holes.

4. Conclusions

Arcing on W surfaces has proven to be a significant erosion mechanism during the Metal Rings Campaign in DIII-D. Arcing was detected by a WI filtered camera and filterscopes and occurred primarily on the shelf ring during ELMs and disruptions. Overall arc damage to the floor ring was negligible in comparison with the shelf. The arcing rate on W surfaces increased with ELM heat flux and had a low threshold $\sim 2 \text{ MW m}^{-2}$, higher on the floor ring than on the shelf. During disruptions, the floor ring was protected from plasma by the shelf and did not have any related arc damage. On the shelf ring, due to different magnetic topology, ELMs and disruptions led to formation of tracks with different pitch angle which could be identified during post mortem analysis. The two causes showed nearly equal contribution to the surface erosion by arcing. Approximately 4% of the shelf W surface was affected by arcing which locally removed about 0.8×10^{21} at. W, an equivalent of a half of total W redeposited outside the metal rings. It is not clear if the W removed by arcing followed the same migration pattern as that atomically eroded, at least a fraction of it was locally redeposited in form of droplets. In the future, it is important to address the effect of fast droplets on core contamination which is expected to be more efficient than by atomically sputtered neutral W.

In summary, a few measures to minimize arcing on W surfaces in a similar experiment in the future can be proposed. The ELM-induced arcing showed very little effect on the floor ring therefore the shelf ring coating has to be similar to the

one on the floor. Also further investigation of the effect of W layer thickness and surface and substrate properties is necessary. It is not clear whether the floor ring coating could perform better than the shelf one during disruptions because of the shadowing. From the general operation safety point of view, disruptions have to be prevented or mitigated which will reduce the related arc damage.

Acknowledgments

This work was supported in part by the US Department of Energy under DE-FG02-07ER54917^a, DE-FC02-04ER54698^b, DE-AC05-00OR22725^c, DE-AC04-94-AL85000^d, DE-SC00013911^e, DE-AC05-07NA27344^f.

ORCID iDs

I Bykov <https://orcid.org/0000-0001-6519-6081>
 C P Chrobak <https://orcid.org/0000-0002-8177-4416>
 T Abrams <https://orcid.org/0000-0002-9605-6871>
 E A Unterberg <https://orcid.org/0000-0003-1353-8865>
 R A Moyer <https://orcid.org/0000-0002-3858-8159>
 J A Boedo <https://orcid.org/0000-0003-2230-4112>
 E T Hinson <https://orcid.org/0000-0001-9713-140X>
 J H Yu <https://orcid.org/0000-0003-0833-5131>

References

- [1] Maeno M *et al* 1980 Mechanism of unipolar arcs in tokamaks *Nucl. Fusion* **20** 1415
- [2] Rudakov D L *et al* 2013 Arcing and its role in PFC erosion and dust production in DIII-D *J. Nucl. Mater.* **438** S805–8 *Supplement Proc. 20th Int. Conf. on Plasma-Surface Interactions in Controlled Fusion Devices*
- [3] Miley G H 1976 Surface effects related to voltage breakdown in CTR devices *J. Nucl. Mater.* **63** 331–6
- [4] Rudakov D L *et al* 2016 Exposures of tungsten nanostructures to divertor plasmas in DIII-D *Phys. Scr.* **2016** 014055
- [5] Tokitani M *et al* 2011 Exfoliation of the tungsten fibreform nanostructure by unipolar arcing in the LHD divertor plasma *Nucl. Fusion* **51** 102001
- [6] Whyte D G *et al* 1997 DiMES divertor erosion experiments on DIII-D *J. Nucl. Mater.* **241** 660–5
- [7] Herrmann A *et al* 2009 Arcing in ASDEX Upgrade with a tungsten first wall *J. Nucl. Mater.* **390391** 747–50 *Proc. 18th Int. Conf. on Plasma-Surface Interactions in Controlled Fusion Device*
- [8] Unterberg E A *et al* Multiple tungsten divertor source, migration and core impact characterization for DIII-D ELM-y H-mode conditions *Phys. Scr.* **T170**
- [9] Unterberg E A *et al* 2016 Overview of the DIII-D divertor tungsten rings campaign *58th Annual Meeting of the APS division of Plasma Physics (31 October–4 November)*
- [10] Luxon J L 2002 A design retrospective of the DIII-D tokamak *Nucl. Fusion* **42** 614
- [11] Wong C P C *et al* 1992 Plasma-surface interactions in controlled fusion devices divertor materials evaluation system at DIII-D *J. Nucl. Mater.* **196** 871–5

- [12] Rudakov D L *et al* 2017 DiMES PMI research at DIII-D in support of ITER and beyond *Fusion Eng. Des.* (<https://doi.org/10.1016/j.fusengdes.2017.03.007>)
- [13] Abrams T *et al* 2017 The inter-ELM tungsten erosion profile in DIII-D H-mode discharges and benchmarking with ERO. OEDGE modeling *Nucl. Fusion* **57** 056034
- [14] Abrams T *et al* 2017 Advances in low-temperature tungsten spectroscopy capability to quantify DIII-D divertor erosion *IEEE Transactions on Plasma Science*
- [15] Mayer M *et al* 2009 Tungsten erosion and redeposition in the all-tungsten divertor of ASDEX Upgrade *Phys. Scr.* **2009** 014039
- [16] Bykov I *et al* Modification of adhered dust on plasma-facing surfaces due to exposure to ELMy H-mode plasma in DIII-D *J. Nucl. Mater. Energy* accepted (<https://doi.org/10.1016/j.nme.2017.05.006>)
- [17] Jüttner B 2001 Cathode spots of electric arcs *J. Phys. D: Appl. Phys.* **34** R103
- [18] Wolff H 1991 Arcing in magnetic fusion devices atomic and plasma-material interaction data for fusion *Nucl. Fusion* **1** (Suppl.) 91
- [19] Guterl J *et al* 2017 Dynamic control of low-Z material deposition and tungsten erosion by strike point sweeping on DIII-D *Nucl. Mater. Energy* (<https://doi.org/10.1016/j.nme.2017.04.017>)
- [20] Stampa A and Kruger H 1983 Simulation experiments on unipolar arcs *J. Phys. D: Appl. Phys.* **16** 2135
- [21] Ertl K, (Asdex Team), Jüttner B 1985 Relevance of plasma-induced arcs for divertor tokamaks *Nucl. Fusion* **25** 1413
- [22] Rohde V *et al* 2011 Tungsten erosion by arcs in ASDEX upgrade *J. Nucl. Mater.* **415** (Suppl. 1) S46–50 *Proc. 19th Int. Conf. on Plasma-Surface Interactions in Controlled Fusion*
- [23] Chrobak C P *et al* 2016 DIII-D first wall metal impurity migration trends *58th Annual Meeting of the APS division of Plasma Physics (31 October–4 November)*
- [24] Gruber O, Lackner K, Pautasso G *et al* 1993 Vertical displacement events and halo currents *Plasma Phys. Control. Fusion* **35** B191
- [25] Lao L L *et al* 2005 MHD equilibrium reconstruction in the DIII-D tokamak *Fusion Sci. Technol.* **48** 968–77
- [26] Baró J, Sempau J, Fernández-Varea J M and Salvat F 1995 Penelope: an algorithm for monte carlo simulation of the penetration and energy loss of electrons and positrons in matter *Nucl. Instrum. Methods Phys. Res. B* **100** 31–46